Title

Rapid and accurate estimation of blood saturation, melanin content, and epidermis thickness from spectral diffuse reflectance.

Journal

Applied optics, 49(10)

ISSN

1539-4522

Authors

Yudovsky, Dmitry
Pilon, Laurent

Publication Date

2010-04-01

DOI

10.1364/AO.49.001707

Peer reviewed

Rapid and Accurate Estimation of Blood Saturation, Melanin Content, and Epidermis Thickness from Spectral Diffuse Reflectance

Dmitry Yudovsky, and Laurent Pilon[§]

University of California, Los Angeles
Henri Samueli School of Engineering and Applied Science
Mechanical and Aerospace Engineering Department
Biomedical Inter-Department Program
Los Angeles, CA 90095-1597
[§] Corresponding Author
Phone: +1 (310)-206-5598, Fax: +1 (310)-206-4830
E-mail: pilon@seas.ucla.edu

December 15, 2010

ABSTRACT

This paper presents a method to determine chromophore concentrations, blood saturation, and epidermal thickness of human skin from diffuse reflectance spectra. Human skin was approximated as a plane-parallel slab of variable thickness supported by a semi-infinite layer corresponding to the epidermis and dermis, respectively. The absorption coefficient was modeled as a function of melanin content for the epidermis and blood content and oxygen saturation for the dermis. The scattering coefficient and refractive index of each layer were found in the literature. Diffuse reflectance spectra between 490 and 620 nm were generated using Monte Carlo simulations for a wide range of melanosome volume fraction, epidermal thickness, blood volume, and oxygen saturation. Then, an inverse method was developed to retrieve these physiologically meaningful parameters from the simulated diffuse reflectance spectra of skin. A previously developed accurate and efficient semi-empirical model for diffuse reflectance of two layered media was used instead of time-consuming Monte Carlo simulations. All parameters could be estimated with relative root mean squared error less than 5% for (i) melanosome volume fraction ranging from 1 to 8%, (ii) epidermal thickness from 20 to 150 μm, (iii) oxygen saturation from 25 to 100%, (iv) blood volume from 1.2 to 10%, and (v) tissue scattering coefficient typical of human skin in the visible part of the

spectrum. Similar approach could be extended to other two-layer absorbing and scattering system.

OCIS codes: 100.3190: Inverse problems, 170.1470: Blood or tissue constituent monitoring, 170.1870: Dermatology, 170.3660: Light propagation in tissues, 170.3880: Medical and biological imaging, 170.6510: Spectroscopy, tissue diagnostics

1 INTRODUCTION

Diffuse reflectance spectroscopy has found many applications in non-invasive monitoring of biological tissues [1–7]. This technique investigates tissue structure, chromophore concentration, and health by measuring the tissue's optical properties. Commercially available devices typically analyze experimental data using the modified Beer-Lambert's law to determine the relative concentrations of tissue chromophores such as melanin, blood, water, or hemoglobin in arbitrary units [6, 8–13]. However the tissue scattering coefficient cannot be retrieved [10, 14]. Alternatively, diffuse reflectance data processed with the diffusion approximation [15] can yield absolute chromophore concentration and measure the tissue's scattering coefficient [16] which is related to tissue microstructure [16–19]. However, this technique requires emitter-detector separation up to 1 cm thus limiting the spatial resolution of these devices [20, 21].

Current spectroscopic techniques are based on the assumption that tissue is homogeneous and that properties are independent of depth [6, 7, 9, 11, 22, 23]. In reality, most bodily organs such as skin, the intestine, or the cervix are protected by a thin lining called the epithelial layer [24]. While the organ is typically composed of connective tissues and perfused with blood vessels and nerves, the protective epithelial layer is bloodless and consists of structured cell layers [24]. Differences in cellular structure and chemical composition give rise to distinct optical properties making the assumption of tissue homogeneity questionable [25]. In skin, for example, the outer epidermal layer is pigmented by melanin which absorbs strongly in the UV while the inner dermal layer is pigmented by blood which absorbs in the visible and near-infrared parts of the spectrum [26]. Furthermore, the thickness of the epidermal layer may vary with anatomical location, gender, and age [27–29].

Multi-layer optical models of tissue have been developed [13, 30–32] to study the effects of tissue structure and chromophore distribution on light propagation. However, such models are computationally intensive and cannot be used in real-time clinical applications [33]. Semi-empirical models of light transfer have been developed to accelerate computation without significant loss of accuracy [34–38]. Mantis and Zonios [34], for example, developed a semi-empirical model for diffuse reflectance of two-layer media. They used their model in an inverse method to determine the optical properties of two-layer tissue phantoms of variable epithelial thickness. However, their method requires that the bottom layer be scattering but non-absorbing [34] which is not the case for most organs [24, 26]. In addition, Tsumura *et al.* [36] developed a semi-empirical model for diffuse reflectance of two-layer scattering and absorbing media based on the modified Beer-Lambert's law. The authors assumed that the thickness of the top layer was equal to 70 μm [36]. Recently, Yudovsky and Pilon [35] developed a semi-empirical model that predicts the diffuse reflectance of strongly scattering two-layer media. The model accounted for (i) absorption and anisotropic scattering in both

layers, (ii) variable thickness of the top layer, and (iii) internal reflection at the medium/air interface. It was shown to accurately predict the diffuse reflectance of skin [35].

The objective of this study is to develop an inverse method based on our semi-empirical model [35] and to assess its robustness in estimating the scattering coefficients, chromophore concentrations in both epidermis and dermis, and the epidermal thickness from spectral diffuse reflectance of human skin.

2 BACKGROUND

Human Skin

Skin is the largest organ of the human body representing a total surface area of approximately 1.8 m^2 and a total weight of approximately 11 kg for adults [39]. The epidermis and dermis are the two main layers. They are separated by the basement membrane and rest on the subcutaneous fat layer [39]. The topmost layer of the epidermis is called the stratum corneum and is composed of dead cells embedded in a lipid matrix. The rest of the epidermis is mainly composed of keratinocytes, melanocytes, and langerhans [39]. Melanocytes synthesize melanin, the skin protein mainly responsible for skin color. Melanin is contained in organelles know as melanosomes which are distributed throughout the epidermis [39]. Depending on genetic factors and UV light exposure, melanosomes occupy 1 to 43% of the epidermal volume corresponding to lightly or darkly pigmented skin, respectively [40–42]. Epidermal thickness varies with bodily location and ranges between 20 and 150 μm [26, 42–44].

The dermis, located beneath the epidermis, is responsible for the skin's pliability, mechanical resistance and temperature control. It contains touch, pressure, and temperature receptors as well as sebaceous and sweat glands and hair follicles [39]. The dermis is composed of collagen fibers perfused by nerves, capillaries, and blood vessels [26, 45, 46]. The thickness of the dermis ranges between 450 and 650 μm [27,47]. Depending on body location and tissue health, the volume of blood in the dermis ranges between 0.2% and 7% [42,48,49]. Approximately half of the blood volume is occupied by erythrocytes (red blood cells) which are responsible for oxygen transfer from the lungs to the rest of the body [42, 49]. Erythrocytes are composed mainly of hemoglobin molecules which reversibly bind to oxygen molecules in the lungs to form oxyhemoglobin. Hemoglobin is known as deoxyhemoglobin once it has released its oxygen molecules. The ratio of oxyhemoglobin molecules to the total number of hemoglobin molecules in the blood is the so-called oxygen saturation denoted by SO_2. Hemoglobin absorption dominates the total absorption of the dermis in the visible range [26, 39, 46]. Furthermore, the spectral extinction coefficient of oxyhemoglobin differs significantly from that of deoxyhemoglobin. Thus, the color of the dermis depends on the average oxygen saturation of its blood content.

Skin Properties Measurement

Various techniques exist to measure chromophore concentrations and blood saturation of human skin. Commercially available non-invasive, optical devices typically measure these quantities in a small region 1 to 2 cm in diameter and report a device specific melanin

(MI) and erythema (EI) index [40, 50]. The MI corresponds qualitatively to the darkness of skin while EI corresponds to the redness or inflammation of skin. Such devices have been used to predict the risk of melanoma skin cancer [40] and as dosimetry feedback during laser treatment of port-wine stains [51] and acne [52]. Recently, hyperspectral imaging in the visible and near-infrared parts of the spectrum has been used to determine the spatial distribution of oxygen saturation in the human skin [12]. This technique has been applied clinically to study diabetic neuropathy [53] and predict the healing potential of diabetic foot ulcers [4, 54]. Such devices typically assume a homogeneous tissue structure and do not model changes in the scattering coefficient with wavelength, biological state, or from patient to patient. Thus, only relative chromophore concentration in arbitrary units can be reported [10, 12, 13]. Furthermore, epidermal thickness and blood volume cannot be determined [10].

Epidermal thickness varies naturally with age, gender, and body location [27–29, 55]. It may also increase or decrease due to external stimuli. For example, UV exposure of human skin has been shown to increase the thickness of the epidermis in addition to increasing its melanin content [56, 57]. On the other hand, smoking has been shown to decrease epidermal thickness [55]. Epidermal thickness can be measured reliably with punch biopsy whereby a sample of the skin is removed and analyzed *ex vivo* [27, 55, 57]. This invasive technique can be painful and destroys the sample. Alternatively, non-invasive measurements of epidermal thickness can be made with techniques such as optical coherent tomograph or ultrasound [58,59]. However, these techniques are primarily sensitive to the tissue's scattering coefficient therefore simultaneous determination of chromophore concentration is difficult [60, 61].

The Radiative Transfer Equation

Biological tissues such as skin are generally absorbing and strongly scattering media [33]. Light transfer through such turbid media is governed by the radiative transfer equation (RTE) written as [15]

$$\hat{\mathbf{s}} \cdot \nabla I(\hat{\mathbf{r}}, \hat{\mathbf{s}}, \lambda) = -\mu_a(\lambda) I(\hat{\mathbf{r}}, \hat{\mathbf{s}}, \lambda) - \mu_s(\lambda) I(\hat{\mathbf{r}}, \hat{\mathbf{s}}, \lambda) + \frac{\mu_s(\lambda)}{4\pi} \int_{4\pi} I(\hat{\mathbf{r}}, \hat{\mathbf{s}}_i, \lambda) \Phi(\hat{s}_i, \hat{s}, \lambda) \mathrm{d}\Omega_i \quad (1)$$

where $I(\hat{\mathbf{r}}, \hat{\mathbf{s}}, \lambda)$ is the spectral intensity at location $\hat{\mathbf{r}}$ in a unit solid angle $\mathrm{d}\Omega$ around direction $\hat{\mathbf{s}}$ expressed in W/cm^2·sr·nm. The linear spectral absorption and scattering coefficients are denoted by $\mu_a(\lambda)$ and $\mu_s(\lambda)$, respectively and are expressed in cm^{-1} while the scattering phase function is denoted by $\Phi(\hat{s}, \hat{s}_i, \lambda)$. The Henyey-Greenstein scattering phase function is an approximate expression that accounts for the anisotropic nature of scattering and is given by [62],

$$\Phi(\hat{s}_i, \hat{s}, \lambda) = \frac{1 - g(\lambda)}{[1 + g(\lambda)^2 - 2g(\lambda)\cos\Theta]^{3/2}} \quad (2)$$

where Θ is the angle between $\hat{s}$ and $\hat{s}_i$ and $g(\lambda)$ is the Henyey-Greenstein asymmetry factor used extensively in tissue optics [33,63,64]. The values of $g(\lambda)$ measured for the epidermis and dermis were approximately the same and ranges between 0.73 and 0.82 in the visible range [46]. In order to account for the magnitude and anisotropy of the scattering phenomenon,

the transport single scattering albedo $\omega_{tr}(\lambda)$ is defined as [15],

$$\omega_{tr}(\lambda) = \frac{\mu_{s,tr}(\lambda)}{\mu_{s,tr}(\lambda) + \mu_a(\lambda)} = \frac{\mu_s(\lambda)[1 - g(\lambda)]}{\mu_s(\lambda)[1 - g(\lambda)] + \mu_a(\lambda)} \tag{3}$$

where, $\mu_{s,tr}(\lambda) = \mu_s(\lambda)[1 - g(\lambda)]$ is the transport scattering coefficient.

Monte Carlo simulation is a stochastic method for solving differential equations such as the RTE [15,32] and has been applied to study of light transfer in skin [23,31,37,65]. To do so, a stochastic model is constructed such that the expected value of a certain random variable is equivalent to the value of physical quantity that is determined by the exact differential equation [66]. The expected value is estimated by sampling the random variable multiple times. In effect, by repeating the simulation, the variance of the estimate diminishes. Thus, albeit at the cost of time, the solution may be found with arbitrary accuracy by increasing the number of simulations [32, 66].

Semi-Empirical Model of Diffuse Reflectance

Recently, Yudovsky and Pilon [35] developed an approximate expression for the diffuse reflectance of skin treated as a two-layer media and given by,

$$R_e = R^*[R_-(n_1, \omega_{tr,epi}) - R_-(n_1, \omega_{tr,derm})] + R_-(n_1, \omega_{tr,derm}) \tag{4}$$

where $\omega_{tr,epi}$ and $\omega_{tr,derm}$ are the transport single scattering albedos of the epidermis and dermis, respectively, while n_1 is the index of refraction of both layers. The reduced reflectance R^* is a function of a single semi-empirical parameter α and expressed as [35],

$$R^* = \frac{\tanh(Y_{epi})}{1/\alpha + (1 - 1/\alpha)\tanh(Y_{epi})} \tag{5}$$

The parameter Y_{epi} is the modified optical thickness defined as $Y_{epi} = \zeta(\mu_{a,epi} + \mu_{s,tr})L_{epi}$, where L_{epi} is the physical thickness of the epidermis [67]. The parameter ζ was approximated by a third order polynomial [35],

$$\zeta^2 = \frac{47}{52} + \frac{31}{49}\omega_{tr,epi} - \frac{49}{54}\omega_{tr,epi}^2 - \frac{17}{27}\omega_{tr,epi}^3 \tag{6}$$

Similarly, assuming the refractive index of tissue to be $n_1 = 1.44$, the semi-empirical parameter α was found to be [35],

$$1/\alpha \;=\; -0.569\omega_{tr,derm}^2 - 0.055\omega_{tr,derm} + 0.993 \tag{7}$$

The function $R_-(n_1, \omega_{tr})$ appearing in Equation (4) is the diffuse reflectance of a semi-infinite homogeneous layer, with transport single scattering albedo ω_{tr} and index of refraction n_1 given by [35],

$$R_-(n_1, \omega_{tr}) = [1 - \rho_{01}(n_1)][1 - \hat{\rho}_{10}(n_1, \omega_{tr})]\frac{\hat{R}_d(\omega_{tr})}{1 - \hat{\rho}_{10}(n_1, \omega_{tr})\hat{R}_d(\omega_{tr})} \tag{8}$$

where $\rho_{01}(n_1)$ is the normal-normal reflectivity of the tissue/air interface defined as,

$$\rho_{01}(n_1) = \left(\frac{n_1 - n_0}{n_1 + n_0}\right)^2 \tag{9}$$

Expressions for $\hat{\rho}_{10}$ and $\hat{R}_d$ were given in Equations (26) and (27) of Ref. [35], respectively. The relative error between the semi-empirical model and Monte Carlo simulations was typically around 3% and never more than 8% for the optical properties of skin in the visible [35].

3 METHODS

Assumptions

Figure 1 shows the two-layer medium considered to approximate skin structure. It consisted

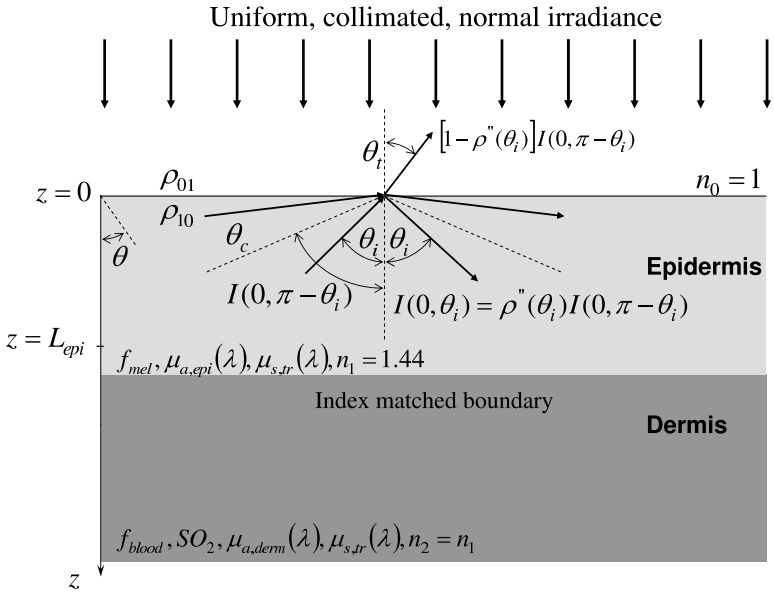

Figure 1: Simplified skin geometry, biological properties, and optical characteristics of the epidermis and dermis considered in this study.

of a plane-parallel slab of thickness L_{epi} representing the epidermis characterized by $\mu_{a,epi}(\lambda)$ and $\mu_{s,tr}(\lambda)$ and index of refraction n_1. This top layer was supported by a semi-infinite sublayer representing the dermis and characterized by $\mu_{a,derm}(\lambda)$, $\mu_{s,tr}(\lambda)$ and n_2. The indices of refraction of both layers were assumed to be identical and constant with wavelength and depth (i.e., $n_1 = n_2$) [63]. The physical distance from the surface was denoted by z. The thickness of epidermis L_{epi} was considered between 20 and 150 μm. The incident light source was modeled as a collimated, monochromatic, and normally incident beam of infinite radius and intensity $I_0(\lambda) = q_0(\lambda)\delta(\theta)$. The quantity $q_0(\lambda)$ denotes the radiative flux of the collimated beam and $\delta(\theta)$ is the Dirac delta function. The air/epidermis interface and

the interface between the slab and the semi-infinite sub-layer were assumed to be optically smooth and therefore specularly reflecting. Then, radiative transfer can be considered as one-dimensional [15, 68]. Thus, the local intensity depends only on depth z and angle θ, i.e., $I(\hat{\mathbf{r}}, \hat{\mathbf{s}}, \lambda) = I(z, \theta, \lambda)$ [15].

Closure Laws

In order to solve the RTE along with the associated boundary conditions [35] using the Monte Carlo method [32], the radiation properties of both the epidermis and dermis must be specified on a spectral basis.

Reduced Scattering Spectrum

The reduced scattering coefficients of the epidermis and dermis were assumed to be equal and given by the power law [33],

$$\mu_{s,tr}(\lambda) = C\left(\frac{\lambda}{\lambda_0}\right)^{-b} \tag{10}$$

where $\lambda_0 = 1$ nm was introduced to ensure consistency in units. This approximate relationship is based on analytical [19, 69–72] and experimental [17, 73, 74] studies of scattering in biological media and has been used to model tissue scattering in the visible and near-infrared parts of the spectrum. It has been shown experimentally that C and b depend on the average size of the microscopic features such as cells or connective tissue responsible for light scattering in the skin [17, 70].

Epidermis

Absorption in the epidermis is mainly due to melanin and flesh. Thus, the absorption coefficient in the epidermal layer $\mu_{a,epi}(\lambda)$ was expressed as [42],

$$\mu_{a,epi}(\lambda) = \mu_{a,mel}(\lambda) f_{mel} + \mu_{a,back}(\lambda)(1 - f_{mel}) \tag{11}$$

where f_{mel} is the volume fraction of melanosomes and $\mu_{a,back}(\lambda)$ is the background absorption of human flesh given by [42, 75],

$$\mu_{a,back}(\lambda) = 7.84 \times 10^8 \lambda^{-3.255} \tag{12}$$

The absorption coefficient of melanosomes as a function of wavelength has been approximated as [76],

$$\mu_{a,mel}(\lambda) = 6.60 \times 10^{11} \lambda^{-3.33} \tag{13}$$

where λ and $\mu_{a,mel}(\lambda)$ are expressed in nanometers and cm^{-1}, respectively. Figure 2a shows $\mu_{a,back}$ and $\mu_{a,mel}$ predicted by Equations (12) and (13) as a function of wavelength between 450 and 700 nm. It illustrates that melanin absorption of UV light is much stronger than the near-infrared light. Indeed, the primary function of melanin is to protect the human body from harmful UV radiation [40–42].

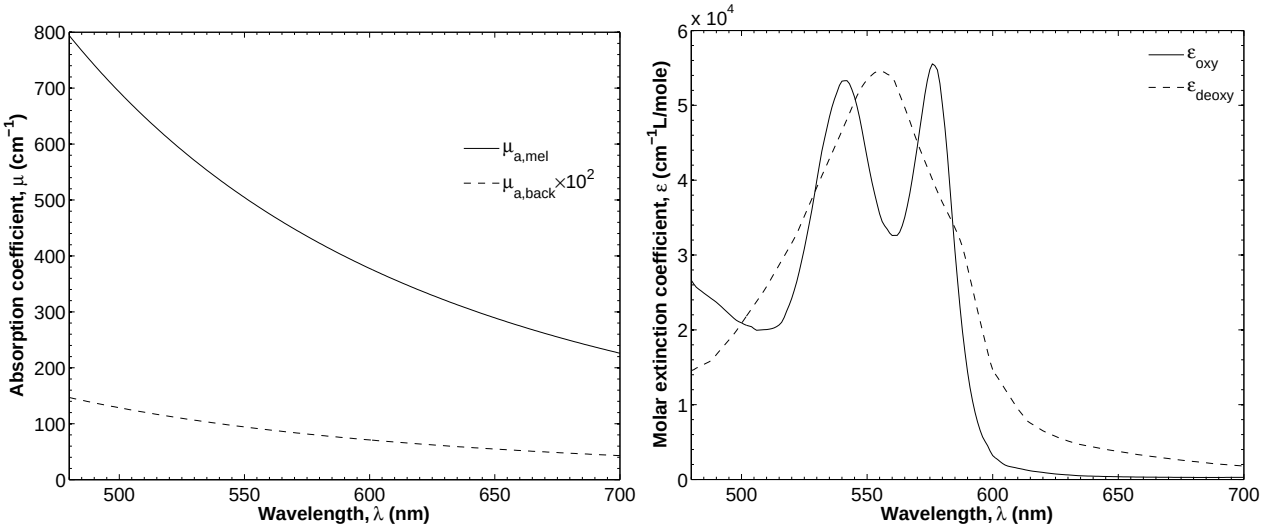

(a) (b)

Figure 2: Absorption properties of endogenous skin chromophores in the visible range (480 to 700 nm). (a) Absorption coefficient of melanosomes [76]. (b) Spectral molar extinction coefficient of human oxyhemoglobin and deoxyhemoglobin [77].

Dermis

The absorption coefficient of the dermis is determined primarily by the absorption of blood [26, 39, 46] and can be written as [48, 77],

$$\mu_{a,derm}(\lambda) = f_{blood}\mu_{a,blood}(\lambda) + \mu_{a,back}(\lambda)(1 - f_{blood}) \tag{14}$$

where f_{blood} is the volume fraction of the dermis occupied by blood and $\mu_{a,back}(\lambda)$ is given by Equation (12). In the visible range, oxyhemoglobin and deoxyhemoglobin are mainly responsible for blood absorption, i.e., $\mu_{a,blood}(\lambda) = \mu_{a,oxy}(\lambda) + \mu_{a,deoxy}(\lambda)$. The absorption coefficient of oxyhemoglobin is given by [48, 77],

$$\mu_{a,oxy}(\lambda) = \epsilon_{oxy}(\lambda)C_{heme}SO_2/66,500 \tag{15}$$

where $\epsilon_{oxy}(\lambda)$ is the molar extinction coefficient of oxyhemoglobin in $\text{cm}^{-1}/(\text{mole/L})$ of molecular weight 66,500 g/mole while C_{heme} is the concentration ratio of hemoglobin in blood [g/L], and SO_2 is the oxygen saturation. Similarly, the absorption coefficient of deoxyhemoglobin is given by [48, 77],

$$\mu_{a,deoxy}(\lambda) = \epsilon_{deoxy}(\lambda)C_{heme}(1 - SO_2)/66,500 \tag{16}$$

where $\epsilon_{deoxy}(\lambda)$ is the molar extinction coefficient of deoxyhemoglobin. While the blood volume fraction f_{blood} and oxygen saturation SO_2 may vary with location and metabolic state, the average value of hemoglobin concentration C_{heme} is typically constant and equal to 150 g/L [44, 77, 78]. The spectral molar extinction coefficients of oxyhemoglobin and

deoxyhemoglobin are available in the literature for a wide range of wavelengths [77, 79–81]. Figure 2b shows the values of $\epsilon_{oxy}(\lambda)$ and $\epsilon_{deoxy}(\lambda)$ used in this study in the visible range from 450 to 700 nm as reported in the literature [77]. Oxyhemoglobin exhibits two absorption peaks at 542 and 578 nm while deoxyhemoglobin exhibits a single peak at 554 nm. Furthermore, oxyhemoglobin is nearly transparent for wavelengths above 600 nm, giving oxygen rich blood its red color.

Simulated Diffuse Reflectance

The biological properties required to estimate the radiative properties of skin in order to solve the RTE can be represented by the input property vector,

$$\vec{a}_i = \langle f_{mel}, L_{epi}, f_{blood}, SO_2, C, b \rangle \tag{17}$$

For a given vector $\vec{a}_i$, the absorption and scattering coefficients of the epidermis and dermis were determined as a function of wavelength using Equations (10) through (16). Then, the RTE was solved on a spectral basis for 40 evenly spaced wavelengths between 480 and 650 nm using the Monte Carlo simulation software developed by Wang and Jacques [32]. A complete and detailed description of the implementation and theoretical underpinnings of this software is given in Ref. [32]. The number of simulated photon packets per simulation was adjusted until the variance associated with the estimate of the diffuse reflectance fell below 1%. Each Monte Carlo simulation was allowed to run with 1,000,000 photon bundles which effectively reduced the variance of the simulated diffuse reflectance spectra to zero. The computed diffuse reflectance is referred to as the "simulated diffuse reflectance spectrum" denoted by $R_i(\vec{a}_i, \lambda_j)$ where λ_j is the j^{th} wavelength and j is an integer between 1 to K.

Inverse Method

The goal of the inverse problem was to estimate the vector $\vec{a}_i$ from the simulated diffuse reflectance $R_i(\vec{a}_i, \lambda_j)$. This was achieved by finding an estimate vector $\vec{a}_e$ that minimizes the sum of the squared residuals δ expressed as,

$$\delta = \sum_{i=1}^{K} [R_i(\vec{a}_i, \lambda_j) - R_e(\vec{a}_e, \lambda_j)]^2 W_j^2 \tag{18}$$

where $R_e(\vec{a}_e, \lambda_j)$ is the estimated spectral diffuse reflectance predicted by Equations (4) and (5), and W_j is the weight associated with the j^{th} residual, and K is the number of wavelengths considered. The input diffuse reflectance spectra $R_i(\vec{a}_i, \lambda_j)$ were calculated by Monte Carlo simulations for a given input parameter vector $\vec{a}_i$. Diffuse reflectance was predicted at $K = 40$ evenly space wavelengths between 490 and 650 nm. This wavelength range was chosen such that melanin, oxyhemoglobin, and deoxyhemoglobin exhibit distinct and significant absorption (Figures 2a and 2b).

Note that the number of wavelengths considered ($K = 40$) was chosen arbitrarily. Theoretically, six wavelengths are required to retrieve the six unknowns f_{mel}, L_{epi}, f_{blood}, SO_2, C, and b. In practice, more measurements can be made to reduce the effects of experimental uncertainty. Furthermore, wavelengths can be strategically chosen to coincide with the

absorption peaks of oxyhemoglobin and deoxyhemoglobin to increase the inverse method's sensitivity to, for example, SO_2 [13]. The goal of this study, however, was to assess the use of the semi-empirical model [Equation (4)] in predicting $\vec{a}_i$. Therefore K was chosen to be relatively large, yet practically implementable so as to reduce the effects of numerical error and wavelength selection.

The values of W_j were chosen to be 2.0 for $\lambda_j < 600$ nm and 1.0 for $\lambda_j \geq 600$ nm to increase the method's sensitivity to changes in SO_2 observed mainly for $\lambda < 600$ nm. Equation (18) was solved iteratively with the constrained Levenberg-Marquardt algorithm [82]. The values of the estimated property vector $\vec{a}_e$ were constrained between physiologically realistic upper and lower bounds reported in the literature and summarized in Table 1. The minimization was stopped once successive iterations of the algorithm no longer reduced δ by more that 10^{-9}. Furthermore, multiple random initial guesses for $\vec{a}_e$ were attempted to prevent convergence to a local minimum.

Table 1: Lower and upper bound values for biological properties of human skin estimated by the inverse method.

Biological Property	**Symbol**	**Lower Bound**	**Upper Bound**	**Reference**
Volume fraction of melanosomes	f_{mel}	1%	10%	[40–42]
Epidermal thickness	L_{epi}	20 μm	150 μm	[26, 42–44]
Blood volume fraction	f_{blood}	0.2%	7%	[42, 49]
Oxygen saturation	SO_2	0%	100%	
Scattering constant	C	4.0×10^5 cm^{-1}	5.5×10^5 cm^{-1}	[42]
Scattering power constant	b	1.10	1.50	[16, 17, 42]

4 RESULTS AND DISCUSSION

Accuracy of Semi-Empirical Model for Skin

Figure 3 compares the diffuse reflectance spectrum $R_i(\lambda)$ calculated by Monte Carlo simulations to that predicted by Equation (4) for $L_{epi} = 30$ μm and $f_{mel} = 5.0\%$. Two different values for both f_{blood} and SO_2 were explored namely $f_{blood} = 0.41$ and 7% and $SO_2 = 0$ and 100%. The effects of oxygen saturation on the shape of the diffuse reflectance spectrum was most apparent when $f_{blood} = 7.0\%$. Skin with oxygen depleted blood, corresponding to $SO_2 = 0\%$, exhibited the single absorption peak of deoxyhemoglobin at 554 nm while reflectance for $SO_2 = 100\%$ exhibits both oxyhemoglobin absorption peaks at 542 and 578 nm. Furthermore, fully oxygenated blood resulted in 1.5 times more reflective skin for $\lambda > 600$ nm than when blood was deoxygenated. Figure 3 also shows that decreasing the blood volume fraction to $f_{blood} = 0.41\%$ greatly diminished the effects of oxygen saturation on the reflectance spectrum. Then, the oxyhemoglobin and deoxyhemoglobin peaks and changes in reflectance were far more subtle since the absorption coefficient of the dermis predicted by Equation (14) was dominated by $\mu_{a,back}$. Note that it typically took 2 minutes on a 2.66 GHz processor to compute the diffuse reflectance spectrum for 40 discrete wavelengths using

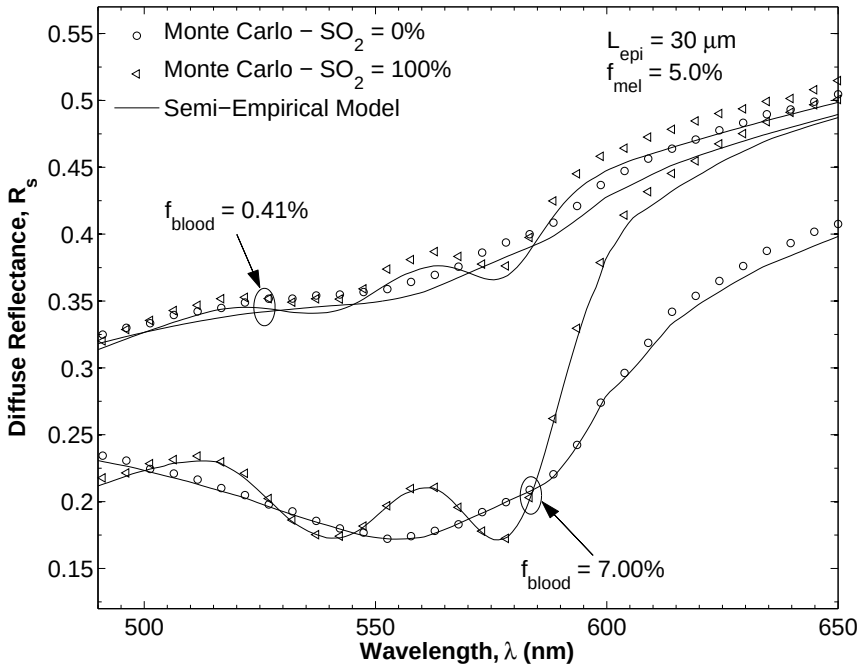

Figure 3: Diffuse reflectance of human skin as a function of wavelength calculated by Monte Carlo simulates and predicted by the semi-empirical model for $L_{epi} = 30$ μm and $f_{mel} = 5.0\%$ and different values of blood volume fraction f_{blood} (0.41 and 7%) and oxygen saturation SO_2 (0 and 100%).

Monte Carlo simulations [32]. On the other hand, the diffuse reflectance spectrum could be estimated nearly instantaneously using Equation (4) to (9).

The accuracy of the semi-empirical model with respect to predictions by Monte Carlo simulations can also be assessed from Figure 3. For $f_{blood} = 7.0\%$, predictions of the diffuse reflectance by the semi-empirical model fell within 3% of that calculated by Monte Carlo simulations for all wavelengths considered. The error was less that 0.5% for λ between 530 and 600 nm, the region associated with the oxyhemoglobin and deoxyhemoglobin peaks. However, for $f_{blood} = 0.41\%$, the semi-empirical model underpredicted the diffuse reflectance by approximately 4% for all wavelengths and for SO_2 equal to 0 and 100%. As discussed by Yudovsky and Pilon [35], the prediction error associated with the semi-empirical model used in this study increased when the transport single scattering albedo of either layer approaches unity. Thus, as f_{blood} decreased, the absorption coefficient of the dermis $\mu_{a,derm}$ decreased and its single scattering albedo approached 1.0 resulting in larger error in the prediction of the diffuse reflectance.

Parameter Estimation

Diffuse reflectance spectra were calculated with Monte Carlo simulations while varying the components of $\vec{a}_i$ between the upper and lower bounds reported in Table 1. Six values of oxygen saturation SO_2, epidermal thickness L_{epi}, melanosome volume fraction f_{mel}, and blood volume fraction f_{blood} and three values of scattering constants C and b were considered

for a total of $11,664$ simulated spectra. For each spectrum, the estimate vector $\vec{a}_e$ was found by minimizing δ defined in Equation (17). To explore the effects of each parameter separately, two scenarios were considered. First, the inverse method's ability to estimate L_{epi}, f_{mel}, f_{blood}, and SO_2 was assessed assuming that the scattering constants C and b were known. Second, the scattering constants C and b were assumed unknown and were retrieved along with the other four input parameters. To assess the accuracy of the inverse method, the root mean squared (rms) error in the retrieval of a given parameter was computed over the entire range of biological properties considered for an arbitrary value of that parameter.

Estimation with Known C and b

In this section, C and b were assumed to be known and equal to $C = 5.0 \times 10^5$ cm^{-1} and $b = 1.30$. These values were measured *ex vivo* for healthy human skin [42]. Here, diffuse reflectance spectra were simulated only for input melanin concentration $f_{mel} = 5\%$. Then, values of f_{mel}, L_{epi}, SO_2, and f_{blood} were retrieved by inverse method using the simulated diffuse reflectance spectrum obtained using Monte Carlo simulations for the range of f_{mel}, L_{epi}, SO_2, and f_{blood} specified in Table 1. The rms relative error between the estimated and input value of $f_{mel} = 5\%$ was less than 0.5% for all values of L_{epi}, SO_2, and f_{blood} considered.

Figures 4a and 4b show the estimated versus input oxygen saturation SO_2 and 10% absolute error bounds for L_{epi} ranging from 20 to 150 μm and for f_{blood} equal to 0.20 and 7.0%, respectively. Figure 4a indicates that SO_2 was overestimated for low values of f_{blood}. This

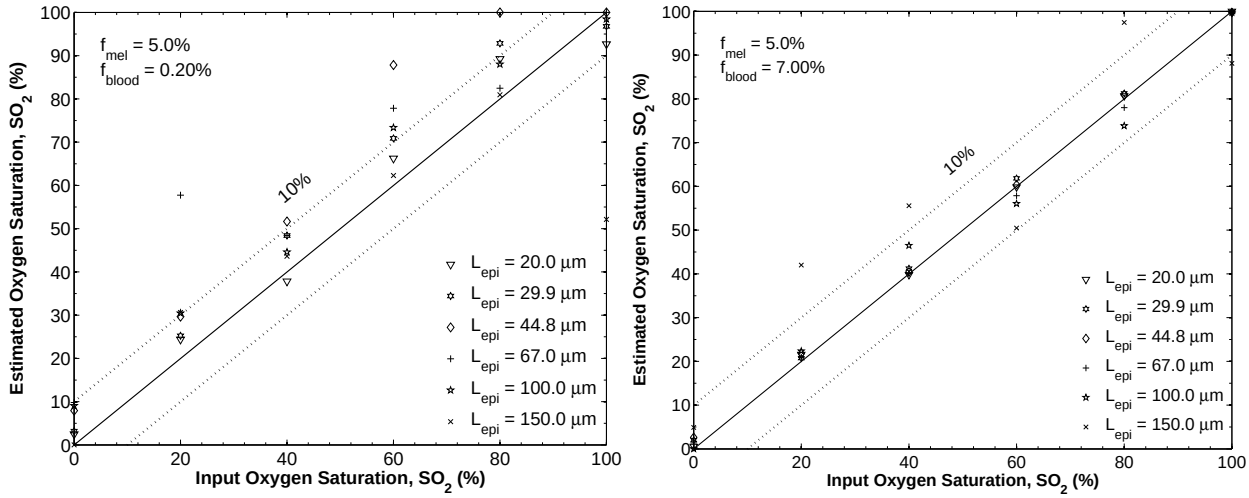

(a) (b)

Figure 4: Estimated versus input oxygen saturation SO_2 and 10% absolute error bounds for input values $f_{mel} = 5.0\%$, $20 \leq L_{epi} \leq 150$ μm, and (a) $f_{blood} = 0.20\%$ and (b) 7%, respectively. The scattering constants were taken as $C = 5.0 \times 10^5$ cm^{-1} and $b = 1.30$.

was primarily due to the underprediction of diffuse reflectance by the semi-empirical model for $\lambda \geq 600$ nm (Figure 3). Indeed, highly oxygenated blood exhibited stronger reflectance in this spectral range. Thus, an overestimate of SO_2 compensated for the inaccuracy of the semi-empirical model. Figure 4a also shows the effect of epidermal thickness on the

prediction of SO_2. A thicker epidermis resulted in poorer estimates of SO_2 since, then, the epidermis optically shielded the dermis. The effect of epidermal thickness on the prediction of SO_2 was best illustrated for input $SO_2 = 60\%$. In this case, when $L_{epi} = 20$ μm, the absolute estimation error was less than 5%. However, for L_{epi} larger than 100 μm, the absolute error in SO_2 increased beyond 10%.

Figure 4b indicates that for blood volume equal to 7.0%, epidermal thickness has little effect on the prediction error associated with SO_2. The rms and the maximum absolute errors between the estimated and input values of SO_2 increased from 2.9 and 9.2% to 13.5 and 47.9%, respectively as L_{epi} increased from 20 to 150 μm. In contrast, as f_{blood} increased from 0.20 to 7.0%, the rms and maximum absolute errors between the estimated and input values of SO_2 decreased from 13.8 to 3% and of 47.9 to 9.4%, respectively. The largest maximum error of 47.9% occurred for the lowest values of f_{blood} and the largest values of L_{epi}. However, it was not typical of this inverse method's performance, as suggested by the rms error.

Nouvong *et al.* [54] recently measured the oxygen saturation near healing and non-healing diabetic foot ulcers using hyperspectral imaging [12]. Their data suggests that skin near non-healing ulcers exhibit a 10% lower oxygen saturation on average when compared with skin near healing ulcers. Furthermore, the values of SO_2 reported were near 55%. The rms error of the present algorithm for $SO_2 = 55\%$ was found to be 3.6%. Thus, the present method is accurate enough to assess wound healing on the diabetic foot.

Figures 5a and 5b show the estimated versus input values of f_{blood} and 0.5% absolute error bounds for $20 \leq L_{epi} \leq 150$ μm and $SO_2 = 0\%$ and 100%, respectively. Unlike

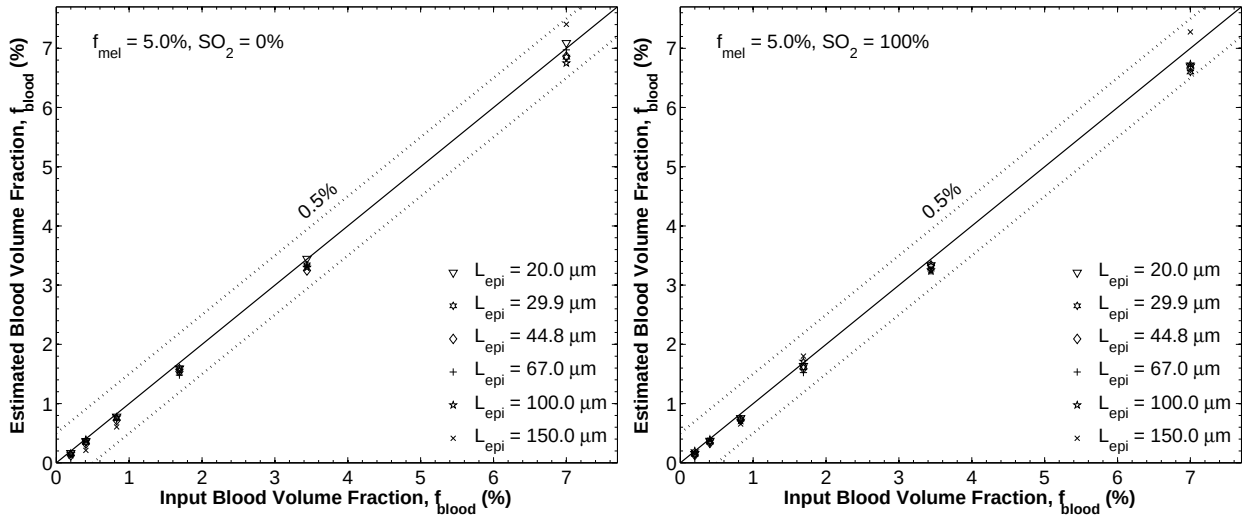

(a) (b)

Figure 5: Estimated versus input blood volume fraction f_{blood} and 0.5% absolute error bounds for input values $f_{mel} = 5.0\%$, $20 \leq L_{epi} \leq 150$ μm, and (a) $SO_2 = 0\%$ and (b) 100%, respectively. The scattering constants were taken as $C = 5.0 \times 10^5$ cm^{-1} and $b = 1.30$.

the estimate of SO_2 previously discussed, the estimate of f_{blood} was almost unaffected by epidermal thickness L_{epi} since the effect of increasing or decreasing f_{blood} was to shift the

entire reflectance spectrum intensity down or up, respectively. Changes in SO_2, on the other hand, affected the spectral shape of the diffuse reflectance spectrum near the absorption peaks of oxyhemoglobin and deoxyhemoglobin ($530 <\leq \lambda <\leq 600$ nm). However, SO_2 had an effect only outside of this wavelength range for larger values of f_{blood}. Thus, the proposed inverse method predicted changes in f_{blood} more accurately than changes in SO_2. Furthermore, as L_{epi} increased from 20 to 150 μm, the rms and the maximum absolute errors between the input and estimated values of f_{blood} increased from 0.074 to 0.21% and 0.30 to 0.71%, respectively. However, these errors remained small and acceptable for all values of L_{epi}.

Figures 6a and 6b show the estimated versus input values of L_{epi} and 10% relative error bounds for SO_2 between 0 and 100% and for $f_{blood} = 0.20$ and 7.0%, respectively. The

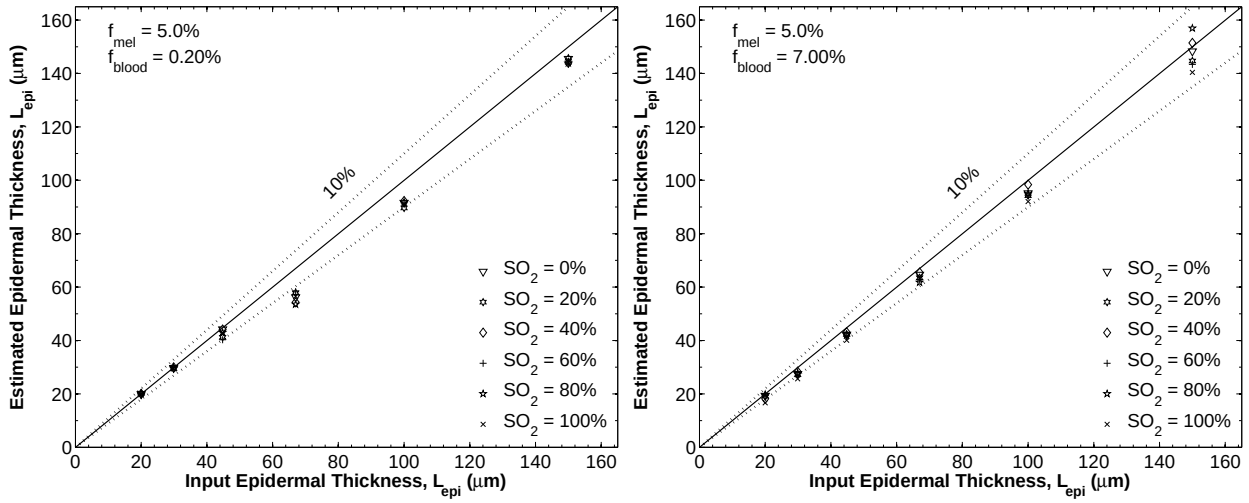

(a) (b)

Figure 6: Estimated versus input epidermal thickness L_{epi} and 10% relative error bounds for input values $f_{mel} = 5.0\%$, $0\% \leq SO_2 \leq 100\%$, and (a) $f_{blood} = 0.20\%$ and (b) 7.0%, respectively. The scattering constants were taken as $C = 5.0 \times 10^5$ cm^{-1} and $b = 1.30$.

relative error in L_{epi} was larger than 10% for f_{blood} less than 1% and L_{epi} between 40 and 100 μm. However, for L_{epi} smaller than 40 μm or larger than 100 μm, the epidermal thickness was dominant in determining the shape of the diffuse reflectance spectrum. In both cases, L_{epi} was estimated accurately for all values of f_{blood}. Indeed, for large values of f_{blood}, $\omega_{tr,derm}$ decreased but remained larger than 0.5 resulting in better agreement between the semi-empirical model and Monte Carlo simulations. Thus, the epidermal thickness L_{epi} was better estimated for larger values of f_{blood}. In fact, as f_{blood} increased from 0.20 to 7.0%, the rms relative error and the maximum relative error between the input and estimated values of L_{epi} decreased from 8.1 to 6.6% and from 20.1 to 16.7%, respectively. Note that for all cases, the maximum absolute error in estimating L_{epi} was less than 14 μm which is approximately the diameter of a keratinocytes cell [83].

Estimation of Melanin Concentration

Here also, C and b were assumed to be known and equal to $C = 5.0 \times 10^5$ cm^{-1} and $b = 1.30$. The value of f_{mel} was varied between 1 and 10% and retrieved by inverse method along with L_{epi}, SO_2, and f_{blood}. While melanosome volume fractions of up to 43% have been reported [42], the range considered in this study was abridged to 10%. Indeed, beyond 10%, the transport single scattering albedo $\omega_{tr,epi}$ became less than 0.50 and the accuracy of the semi-empirical model in predicting the diffuse reflectance greatly diminished [35] making accurate inversion difficult or even impossible.

Figure 7 shows the estimated versus input values of f_{mel} and 0.5% absolute error bounds for various input values of L_{epi} and f_{blood} and for $SO_2 = 50\%$. The estimate of f_{mel} was well

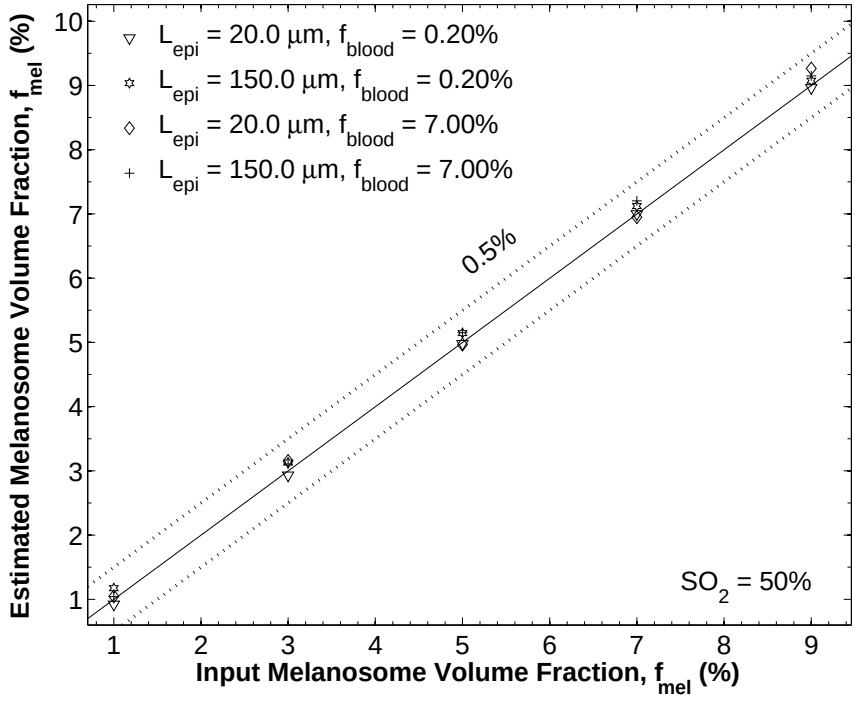

Figure 7: Estimated versus input melanosome volume fraction f_{mel} and 0.5% absolute error bounds for input values $20 \leq L_{epi} \leq 150$ μm and $0.20 \leq f_{blood} \leq 7.0\%$, and $SO_2 = 50\%$. The scattering constants were taken as $C = 5.0 \times 10^5$ cm^{-1} and $b = 1.30$.

within 0.5% for all values of L_{epi}. As with f_{blood} shown in Figure 5, the absolute error was small and acceptable. Similar results as those previously discussed for $f_{mel} = 5\%$ were found for the retrieved values of SO_2, L_{epi} and f_{blood} and need not be repeated. In other words, the ability of the inverse method to estimate L_{epi}, SO_2, and f_{blood} was not altered by the melanosome volume fraction f_{mel}.

Estimation of Tissue Scattering

So far, the values of C and b were considered to be constant and known. In reality, they depend on the average diameter and concentration of collagen fibers in the skin, for example.

They may vary from 4.0×10^5 to 5.5×10^5 cm^{-1} and from 1.1 to 1.5, respectively [17,18,70]. To test the ability of the proposed inverse method to estimate C and b from diffuse reflectance measurements, Monte Carlo simulations were performed while varying C and b between these bounds. Then, δ given by Equation (18) was minimized to find optimal estimates of C and b for each diffuse reflectance spectrum in addition to the four parameters f_{mel}, L_{epi}, f_{blood}, and SO_2. It was found that f_{mel}, L_{epi}, f_{blood}, SO_2, and b or C could be estimated accurately only if C or b was assumed to be known, respectively. However, if both b and C were retrieved simultaneously, only SO_2, f_{mel} and L_{epi} could be estimated reliably while f_{blood}, b, and C could not be accurately estimated. This was despite the fact that the estimated diffuse reflectance by the semi-empirical model using the retrieved parameters matched the input diffuse reflectance closely for all cases considered.

Therefore, values of b measured *in vitro* and reported in the literature [16, 17, 42] were used in conjunction with the present inverse method. Figures 8a and 8b show the estimated versus input scattering constant C and 5% relative error bounds for $20 <\leq L_{epi} <\leq 150$ μm, $0.20\% \leq f_{blood} \leq 7\%$, $f_{mel} = 5\%$ and for $SO_2 = 0$ and 100 %, respectively. The parameter

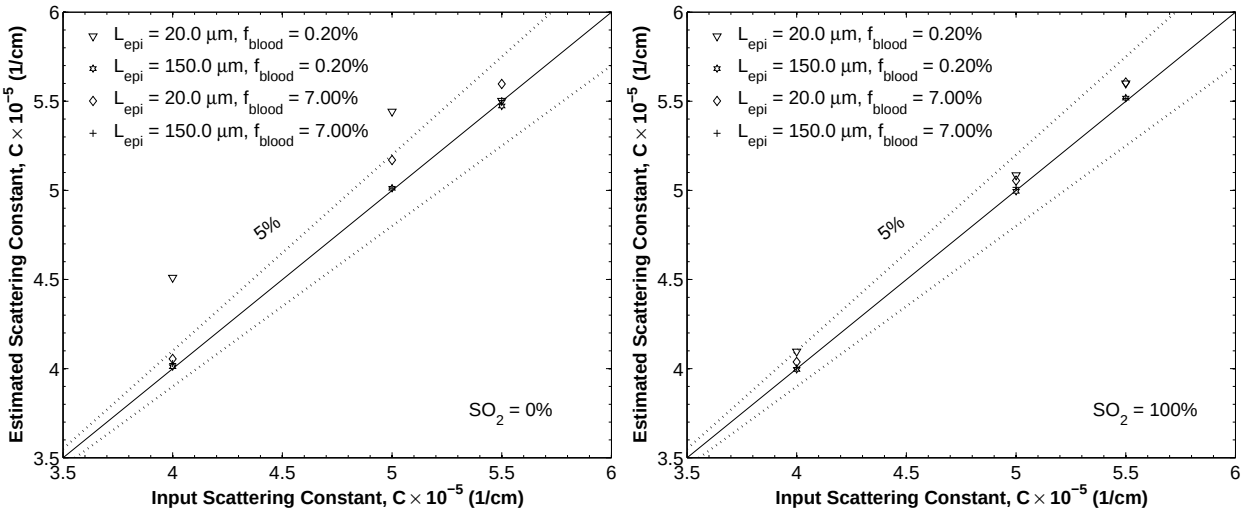

(a) (b)

Figure 8: Estimated versus input scattering constant C and 5% relative error bounds for input values $20 \leq L_{epi} \leq 150$ μm, $0.20 \leq f_{blood} \leq 7.0\%$, $f_{mel} = 5.0\%$, $b = 1.30$ for (a) $SO_2 = 0\%$ and (b) $SO_2 = 100\%$, respectively. The scattering constant b is assumed to be known.

b was assumed to be constant and equal to 1.30 for both simulated and estimated diffuse reflectance. The blood volume fraction f_{blood} had the strongest effect on the relative error in the retrieved C. Greater error was observed for small values of f_{blood} for reasons previously discussed. As f_{blood} increased from 0.20 to 7.0%, the rms relative error and the maximum relative error between the input and estimated value of C decreased from 5.9 to 1.4% and from 23.4 to 3.4%, respectively. These errors remained small and acceptable.

To illustrate the accuracy of the inverse method using the semi-empirical model, simulated diffuse reflectance spectra were produced for $L_{epi} = 50$ and 100 μm and f_{mel} equal to 1%,

5%, and 10% representing weakly, moderately, and strongly pigmented skin, respectively. The input values of the other parameters SO_2, f_{blood}, and C were chosen in the ranges given in Table 1. Then, all 5 parameters were estimated, while b was imposed to be 1.30. Table 2 shows the relative rms error between the input and estimated values of f_{mel}, L_{epi}, f_{blood}, SO_2, and C for the three skin complexions and two epidermal thicknesses considered. Note that input values of SO_2 smaller than 25% were ignored while calculating the relative rms error associated with estimating SO_2 because these small values are unrealistic for living tissues.

Table 2: Relative rms error between retrieved and input values of f_{mel}, L_{epi}, SO_2, f_{blood}, and C for $L_{epi} = 50$ and 100 μm and f_{mel} equal to 1%, 5%, and 10% representing weakly, moderately, and strongly pigmented skin, respectively. The input values of SO_2, f_{blood}, and C were chosen in the ranges given in Table 1. The rms error in estimating SO_2 was calculated for $SO_2 > 25\%$

	$L_{epi} = 50$ μm					$L_{epi} = 100$ μm				
$\mathbf{f_{mel}}$	$\mathbf{f_{mel}}$	$\mathbf{L_{epi}}$	$\mathbf{SO_2}$	$\mathbf{f_{blood}}$	$\mathbf{C}$	$\mathbf{f_{mel}}$	$\mathbf{L_{epi}}$	$\mathbf{SO_2}$	$\mathbf{f_{blood}}$	$\mathbf{C}$
1%	9.3%	16.1%	1.3%	2.5%	2.4%	10.1%	15.4%	4.8%	5.2%	2.2%
5%	9.9%	9.6%	4.6%	10.2%	2.4%	3.7%	5.7%	4.9%	6.4%	2.5%
10%	3.5%	1.8%	3.2%	11.8%	3.1%	0.5%	3.8%	15.8%	11.3%	2.2%

Finally, the present inverse algorithm was recently used to detect callus and ulcer formation on the foot of a diabetic patient [84]. Hyperspectral tissue reflectance images of the foot of a diabetic patient were collected at regular interval for 18 months [54]. During this period a foot ulcer developed on the plantar surface of the left sole [54]. Hyperspectral data of the ulceration site was available 30 days before the ulcer formed. A diabetic foot ulcer is often preceded by callus formation (i.e., epidermal thickening) around the preulcerative site [85,86]. As the ulcer formation progresses, the epidermis immediately above the necrotic tissue diminishes in thickness [85, 86]. Estimation of the epidermal thickness was performed with the present algorithm to confirm that such changes could be detected optically. In fact, the preulcerative site exhibited an epidermal thickness of 85 μm and was surrounded by much thicker epidermis of approximately (130 μm). These results show promise that the present algorithm could be used to assess tissue health *in vivo* and in a clinical setting. However, complete discussion of this topic falls outside the scope of this paper.

5 CONCLUSION

In this paper, human skin was modeled as a slab of variable thickness, corresponding to the epidermis, supported by a semi-infinite layer, corresponding to the dermis. Absorption in the epidermis was due to melanin and varied depending on melanosome volume fraction. Absorption in the epidermis was due to oxyhemoglobin and deoxyhemoglobin and varied with blood volume fraction and oxygen saturation. Index of refraction and scattering coefficient in both layers were assumed to be identical. The radiative transfer equation was solved on a spectral basis between 490 and 650 nm by Monte Carlo simulations to produce

simulated diffuse reflectance spectra for a wide range of biological properties. Then, an inverse method was used to retrieve physiologically meaningful parameters from the simulated diffuse reflectance spectra. A quicker semi-empirical model [35] was used instead of Monte Carlo simulations in the iterative inversion procedure. The accuracy of the inverse method in estimating f_{mel}, L_{epi}, SO_2, f_{blood} and C was explored for a range of physiologically meaningful values specified in Table 1. In summary, all parameters could be estimated with relative rms error less than 5% for f_{mel} between 1 and 8%, L_{epi} ranging from 20 to 150 μm, SO_2 from 25 to 100%, f_{blood} from 1.2 to 10%, and C from 4.0×10^5 to 5.5×10^5 cm^{-1}. The methodology presented can be applied to any two layer optical system where scattering dominates over absorption.

5.1 Acknowledgments

This research was funded in part through a grant from the National Institute of Diabetes and Digestive and Kidney Diseases (R42-DK069871) through HyperMed, Inc.. The authors would like to thank A. Nouvong, K. Schomacker, and R. Lifsitz for useful discussion and exchange of information.

References

[1] G. Zonios, A. Dimou, I. Bassukas, D. Galaris, A. Tsolakidis, and E. Kaxiras, "Melanin absorption spectroscopy: new method for noninvasive skin investigation and melanoma detection", *Journal of Biomedical Optics*, vol. 13, no. 1, pp. 014017, 2008.

[2] W.M. Kuebler, "How NIR is the future in blood flow monitoring?", *Journal of Applied Physiology*, vol. 104, no. 4, pp. 905–906, 2008.

[3] R.L.P. van Veen, A. Amelink, M. Menke-Pluymers, C. van der Pol, and H. Sterenborg, "Optical biopsy of breast tissue using differential path-length spectroscopy", *Physics in Medicine and Biology*, vol. 50, no. 11, pp. 2573–2581, 2005.

[4] L. Khaodhiar, T. Dinh, K.T. Schomacker, S.V. Panasyuk, J.E. Freeman, R. Lew, T. Vo, A.A. Panasyuk, C. Lima, J.M. Giurini, et al., "The use of medical hyperspectral technology to evaluate microcirculatory changes in diabetic foot ulcers and to predict clinical outcomes", *Diabetes Care*, vol. 30, no. 4, pp. 903–910, 2007.

[5] A. Torricelli, D. Contini, A. Pifferi, L. Spinelli, and R. Cubeddu, "Functional brain imaging by multi-wavelength time-resolved near infrared spectroscopy", *Opto-Electronics Review*, vol. 16, no. 2, pp. 131–135, 2008.

[6] N. Tsumura, M. Kawabuchi, H. Haneishi, and Y. Miyake, "Mapping pigmentation in human skin from multi-channel visible spectrum image by inverse optical scattering technique", *Journal of Imaging Science and Technology*, vol. 45, no. 5, pp. 444–450, 2001.

[7] N. Tsumura, H. Haneishi, and Y. Miyake, "Independent-component analysis of skin color image", *Journal of the Optical Society of America A*, vol. 16, no. 9, pp. 2169–2176, 1999.

[8] A Vogel, V.V. Chernomordik, J.D. Riley, M. Hassan, F. Amyot, B. Dasgeb, S.G. Demos, R. Pursley, R.F. Little, R. Yarchoan, T. Tao, and A.H. Gandjbakhche, "Using noninvasive

multispectral imaging to quantitatively assess tissue vasculature", *Journal of Biomedical Optics*, vol. 12, no. 5, pp. 051604, 2007.

[9] N. Tsumura, R. Usuba, K. Takase, T. Nakaguchi, N. Ojima, N. Komeda, and Y. Miyake, "Image-based control of skin translucency", *Applied Optics*, vol. 47, no. 35, pp. 6543–6549, 2008.

[10] L. Kocsis, P. Herman, and A. Eke, "The modified Beer-Lambert law revisited", *Physics in Medicine and Biology*, vol. 51, no. 5, pp. 91–98, 2006.

[11] N. Tsumura, T. Nakaguchi, N. Ojima, K. Takase, S. Okaguchi, K. Hori, and Y. Miyake, "Image-based control of skin melanin texture", *Applied Optics*, vol. 45, no. 25, pp. 6626–6633, 2006.

[12] K.J. Zuzak, M.D. Schaeberle, E.N. Lewis, and I.W. Levin, "Visible reflectance hyperspectral imaging: characterization of a noninvasive, *in-vivo* system for determining tissue perfusion", *Analytical Chemistry*, vol. 74, no. 9, pp. 2021–2028, 2002.

[13] S.J. Matcher, C.E. Elwell, C.E. Cooper, M. Cope, and D.T. Delpy, "Performance comparison of several published tissue near-infrared spectroscopy algorithms", *Analytical Biochemistry*, vol. 227, no. 1, pp. 54–68, 1995.

[14] A. Sassaroli and S. Fantini, "Comment on the modified Beer-Lambert law for scattering media", *Physics in Medicine and Biology*, vol. 49, no. 14, pp. 255–257, 2004.

[15] M.F. Modest, *Radiative Heat Transfer*, Academic Press, San Diego, CA, 2003.

[16] R.M.P. Doornbos, R. Lang, M.C. Aalders, F.W. Cross, and H. Sterenborg, "The determination of in vivo human tissue optical properties and absolute chromophore concentrations using spatially resolved steady-state diffuse reflectance spectroscopy", *Physics in Medicine and Biology*, vol. 44, no. 4, pp. 967–982, 1999.

[17] A.M.K. Nilsson, C. Sturesson, D.L. Liu, and S. Andersson-Engels, "Changes in spectral shape of tissue optical properties in conjunction with laser-induced thermotherapy", *Applied Optics*, vol. 37, no. 7, pp. 1256–1267, 1998.

[18] I.S. Saidi, S.L. Jacques, and F.K. Tittel, "Mie and Rayleigh modeling of visible-light scattering in neonatal skin", *Applied Optics*, vol. 34, no. 31, pp. 7410–7418, 1995.

[19] J.M. Schmitt and G. Kumar, "Optical scattering properties of soft tissue: a discrete particle model", *Applied Optics*, vol. 37, no. 13, pp. 2788, 1998.

[20] R.L.P. van Veen, A. Amelink, M. Menke-Pluymers, C. van der Pol, and H. Sterenborg, "Optical biopsy of breast tissue using differential path-length spectroscopy", *Physics in Medicine and Biology*, vol. 50, no. 11, pp. 2573–2581, 2005.

[21] J.C. Finlay and T.H. Foster, "Hemoglobin oxygen saturations in phantoms and in vivo from measurements of steady-state diffuse reflectance at a single, short source-detector separation", *Medical Physics*, vol. 31, no. 7, pp. 1949–1959, 2004.

[22] E. Okada, M. Firbank, and D.T. Delpy, "The effect of overlying tissue on the spatial sensitivity profile of near-infrared spectroscopy", *Physics in Medicine and Biology*, vol. 40, no. 12, pp. 2093–2108, 1995.

[23] M. Hiraoka, M. Firbank, M. Essenpreis, M. Cope, S.R. Arridge, P. Zee, and D.T. Delpy, "A Monte Carlo investigation of optical pathlength in inhomogeneous tissue and its application to near-infrared spectroscopy", *Physics in Medicine and Biology*, vol. 38, no. 12, pp. 1859–1876, 1993.

[24] H. Gray, *Gray's Anatomy*, pp. 1082–1085, Bounty Books, New York, 1977.

[25] R.J. Hunter, M.S. Patterson, T.J. Farrell, and J.E. Hayward, "Haemoglobin oxygenation of a two-layer tissue-simulating phantom from time-resolved reflectance: effect of top layer thickness", *Physics in Medicine and Biology*, vol. 47, no. 2, pp. 193–208, 2002.

[26] R.R. Anderson and J.A. Parrish, "The optics of human skin", *Journal of Investigative Dermatology*, vol. 77, no. 1, pp. 13–19, 1981.

[27] Y. Lee and K. Hwang, "Skin thickness of Korean adults", *Surgical and Radiologic Anatomy*, vol. 24, no. 3, pp. 183–189, 2002.

[28] M.C. Branchet, S. Boisnic, C. Frances, and A.M. Robert, "Skin thickness changes in normal aging skin", *Gerontology*, vol. 36, no. 1, pp. 28–35, 1990.

[29] D.E. Barker, "Skin thickness in the human", *Plastic and Reconstructive Surgery*, vol. 7, no. 2, pp. 115–116, 1951.

[30] K.M. Katika and L. Pilon, "Steady-state directional diffuse reflectance and fluorescence of human skin", *Applied Optics*, vol. 45, no. 17, pp. 4174–4183, 2006.

[31] H. Zeng, C.E. MacAulay, B. Palcic, and D.I. McLean, "Monte Carlo modeling of tissue autofluorescence measurement and imaging", *Proceedings of the SPIE*, vol. 2135, no. 1, pp. 94–104, 1994.

[32] L. Wang and S.L. Jacques, "Monte Carlo modeling of light transport in multi-layered tissues in standard C", last accessed 3/31/2009, *http://labs.seas.wustl.edu/bme/Wang/mcr5/Mcman.pdf*.

[33] V.V. Tuchin, *Tissue Optics: Light Scattering Methods and Instruments for Medical Diagnosis*, SPIE Press, San Diego, CA, 2007.

[34] G. Mantis and G. Zonios, "Simple two-layer reflectance model for biological tissue applications", *Applied Optics*, vol. 48, no. 18, pp. 3490–3496, 2009.

[35] D. Yudovsky and L. Pilon, "Simple and accurate expressions for diffuse reflectance of semi-infinite and two-layer absorbing and scattering media", *Applied Optics*, vol. 48, no. 35, pp. 6670–6683, 2009.

[36] N. Tsumura, D. Kawazoe, T. Nakaguchi, N. Ojima, and Y. Miyake, "Regression-based model of skin diffuse reflectance for skin color analysis", *Optical Review*, vol. 15, no. 6, pp. 292–294, 2008.

[37] C.M. Gardner, S.L. Jacques, and A.J. Welch, "Light transport in tissue: accurate expressions for one-dimensional fluence rate and escape function based upon Monte Carlo simulation", *Lasers in Surgery and Medicine*, vol. 18, no. 2, pp. 129–138, 1996.

[38] J. Wu, F. Partovi, M.S. Field, and R.P. Rava, "Diffuse reflectance from turbid media: an analytical model of photon migration", *Applied Optics*, vol. 32, no. 7, pp. 1115–1121, 1993.

[39] A.R. Young, "Chromophores in human skin", *Physics in Medicine and Biology*, vol. 42, no. 5, pp. 789–802, 1997.

[40] T. Dwyer, G. Prota, L. Blizzard, R. Ashbolt, and M.R. Vincensi, "Melanin density and melanin type predict melanocytic naevi in 19-20 year olds of northern European ancestry", *Melanoma Research*, vol. 10, no. 4, pp. 387–394, 2000.

[41] T. Dwyer, H.K. Muller, L. Blizzard, R. Ashbolt, and G. Phillips, "The use of spectrophotometry to estimate melanin density in Caucasians", *Cancer Epidemiology Biomarkers & Prevention*, vol. 7, no. 3, pp. 203–206, 1998.

[42] S.L. Jacques, "Origins of tissue optical properties in the UVA, visible, and NIR regions", in *Advances in Optical Imaging and Photon Migration*, R.R. Alfano and J.G. Fujimoto, Eds., vol. 2, pp. 364–370. Optical Society of America, Washington, DC, 1996.

[43] M. Doi and S. Tominaga, "Spectral estimation of human skin color using the kubelka-munk theory", in *Color Imaging VIII: Processing, Hardcopy, and Applications*, R. Eschbach and G.G. Marcu, Eds., vol. 5008, pp. 221–228. SPIE, 2003.

[44] R. Flewelling, "Noninvasive optical monitoring", in *The Biomedical Engineering Handbook*, J Bronzion, Ed., pp. 1–11. IEEE Press, Boca Rotan, FL, 1981.

[45] I.V. Meglinski and S.J. Matcher, "Modeling of skin reflectance spectra", in *Proceedings of the SPIE*, 2001, vol. 4241, pp. 78–87.

[46] M.J.C. Van Gemert, A.J. Welch, W.M. Star, M. Motamedi, and W.F. Cheong, "Tissue optics for a slab geometry in the diffusion approximation", *Lasers in Medical Science*, vol. 2, no. 4, pp. 295–302, 1987.

[47] W.F. Southwood, "The thickness of the skin", *Plastic and Reconstructive Surgery*, vol. 15, no. 5, pp. 423–429, 1955.

[48] A. Krishnaswamy and G.V.G. Baranoski, "A biophysically-based spectral model of light interaction with human skin", in *Computer Graphics Forum*. Blackwell Publishing, Inc, 2004, vol. 23, pp. 331–340.

[49] E. Angelopoulou, "Understanding the color of human skin", *Human Vision and Electronic Imaging VI*, vol. 4299, no. 1, pp. 243–251, 2001.

[50] P. Clarys, K. Alewaeters, R. Lambrecht, and AO Barel, "Skin color measurements: comparison between three instruments: the Chromameter®, the DermaSpectrometer® and the Mexameter®", *Skin Research and Technology*, vol. 6, no. 4, pp. 230–238, 2000.

[51] Kono, T. and Erçöçen, A.R. and Nakazawa, H. and Honda, T. and Hayashi, N. and Nozaki, M., "The flashlamp-pumped pulsed dye laser (585 nm) treatment of hypertrophic scars in Asians", *Annals of Plastic Surgery*, vol. 51, no. 4, pp. 366–371, 2003.

[52] H.J. Yoon, D.H. Lee, S. Ok Kim, K. Chan Park, and S. Woong Youn, "Acne erythema improvement by long-pulsed 595-nm pulsed-dye laser treatment: A pilot study", *Journal of Dermatological Treatment*, vol. 19, no. 1, pp. 38–44, 2008.

[53] R.L. Greenman, S. Panasyuk, X. Wang, T.E. Lyons, T. Dinh, L. Longoria, J.M. Giurini, J. Freeman, L. Khaodhiar, and A. Veves, "Early changes in the skin microcirculation and muscle metabolism of the diabetic foot", *The Lancet*, vol. 366, no. 9498, pp. 1711–1717, 2005.

[54] A. Nouvong, B. Hoogwerf, E. Mohler, B. Davis, A. Tajaddini, and E. Medenilla, "Evaluation of diabetic foot ulcer healing with hyperspectral imaging of oxyhemoglobin and deoxyhemoglobin", *Diabetes Care*, vol. 32, no. 11, 2009.

[55] J. Sandby-Moller, T. Poulsen, and H.C. Wulf, "Epidermal thickness at different body sites: relationship to age, gender, pigmentation, blood content, skin type and smoking habits", *Acta Dermato-Venereologica*, vol. 83, no. 6, pp. 410–413, 2003.

[56] T. Gambichler, J. Huyn, N.S. Tomi, G. Moussa, C. Moll, A. Sommer, P. Altmeyer, and K. Hoffmann, "A comparative pilot study on ultraviolet-induced skin changes assessed by noninvasive imaging techniques *in vivo*", *Photochemistry and Photobiology*, vol. 82, no. 4, pp. 1103–1107, 2006.

[57] J. Lock-Andersen, P. Therkildsen, O.F. de Fine, M. Gniadecka, K. Dahlstrøm, T. Poulsen, and HC Wulf, "Epidermal thickness, skin pigmentation and constitutive photosensitivity.", *Photodermatology, Photoimmunology & Photomedicine*, vol. 13, no. 4, pp. 153–157, 1997.

[58] T. Gambichler, R. Matip, G. Moussa, P. Altmeyer, and K. Hoffmann, "In vivo data of epidermal thickness evaluated by optical coherence tomography: effects of age, gender, skin type, and anatomic site", *Journal of Dermatological Science*, vol. 44, no. 3, pp. 145–152, 2006.

[59] P.P. Guastalla, V.I. Guerci, A. Fabretto, F. Faletra, D.L. Grasso, E. Zocconi, D. Stefanidou, P. D'Adamo, L. Ronfani, M. Montico, et al., "Detection of epidermal thickening in GJB2 carriers with epidermal US", *Radiology*, vol. 251, no. 1, pp. 280–286, 2009.

[60] D.J. Faber and T.G. van Leeuwen, "Are quantitative attenuation measurements of blood by optical coherence tomography feasible?", *Optics Letters*, vol. 34, no. 9, pp. 1435–1437, 2009.

[61] D.J. Faber, E.G. Mik, M.C.G. Aalders, and T.G. van Leeuwen, "Toward assessment of blood oxygen saturation by spectroscopic optical coherence tomography", *Optics Letters*, vol. 30, no. 9, pp. 1015–1017, 2005.

[62] L.G. Henyey and J.L. Greenstein, "Diffuse radiation in the galaxy", *Annales d'Astrophysique*, vol. 93, pp. 70–83, 1940.

[63] M.J.C. Van Gemert, S.L. Jacques, H. Sterenborg, and W.M. Star, "Skin optics", *IEEE Transactions on Biomedical Engineering*, vol. 36, no. 12, pp. 1146–1154, 1989.

[64] S.L. Jacques, C.A. Alter, and S.A. Prahl, "Angular dependence of HeNe laser light scattering by human dermis", *Lasers in the Life Sciences*, vol. 1, no. 4, pp. 309–333, 1987.

[65] S.K. Chang, D. Arifler, R. Drezek, M. Follen, and R. Richards-Kortum, "Analytical model to describe fluorescence spectra of normal and preneoplastic epithelial tissue: comparison with Monte Carlo simulations and clinical measurements", *Journal of Biomedical Optics*, vol. 9, no. 3, pp. 511–522, 2004.

[66] I. Lux and L. Koblinger, *Monte Carlo Particle Transport Methods: Neutron and Photon Calculations*, CRC Press, Boca Raton, FL, 6^{th} edition, 1991.

[67] M.J.C. van Gemert and W.M. Star, "Relations between the Kubelka-Munk and the transport equation models for anisotropic scattering", *Lasers in the Life Sciences*, vol. 1, no. 98, pp. 287–298, 1987.

[68] M. Keijzer, S.L. Jacques, S.A. Prahl, and A.J. Welch, "Light distributions in artery tissue: Monte Carlo simulations for finite-diameter laser beams", *Lasers Surgery in Medicine*, vol. 9, no. 2, pp. 148–154, 1989.

[69] S.Y. Shchyogolev, "Inverse problems of spectroturbidimetry of biological disperse systems: an overview", *Journal of Biomedical Optics*, vol. 4, no. 4, pp. 490–503, 1999.

[70] J.R. Mourant, J.P. Freyer, A.H. Hielscher, A.A. Eick, D. Shen, and T.M. Johnson, "Mechanisms of light scattering from biological cells relevant to noninvasive optical-tissue diagnostics", *Applied Optics*, vol. 37, no. 16, pp. 3586–3593, 1998.

[71] J.R. Mourant, T. Fuselier, J. Boyer, T.M. Johnson, and I.J. Bigio, "Predictions and measurements of scattering and absorption over broad wavelength ranges in tissue phantoms", *Applied Optics*, vol. 36, no. 4, pp. 949–957, 1997.

[72] R. Graaff, J.G. Aarnoudse, J.R. Zijp, P.M.A. Sloot, F.F.M. de Mul, J. Greve, and M.H. Koelink, "Reduced light-scattering properties for mixtures of spherical particles: a simple approximation derived from Mie calculations", *Applied Optics*, vol. 31, no. 10, pp. 1370–1376, 1992.

[73] A.N. Bashkatov, E.A. Genina, V.I. Kochubey, and V.V. Tuchin, "Optical properties of human skin, subcutaneous and mucous tissues in the wavelength range from 400 to 2000 nm", *Journal of Physics D: Applied Physics*, vol. 38, no. 15, pp. 2543–2555, 2005.

[74] G. Vargas, E.K. Chan, J.K. Barton, and A.J. Welch, "Use of an agent to reduce scattering in skin", *Lasers in Surgery and Medicine*, vol. 24, no. 2, pp. 133–141, 1999.

[75] I.S. Saidi, *Transcutaneous Optical Measurement of Hyperbilirubinemia in Neonates*, PhD thesis, Rice University, 1992.

[76] S.L. Jacques and D.J. McAuliffe, "The melanosome: threshold temperature for explosive vaporization and internal absorption coefficient during pulsed laser irradiation", *Photochemistry and Photobiology*, vol. 53, no. 6, pp. 769–775, 1991.

[77] S. Prahl, "Optical absorption of hemoglobin", World Wide Web: http://omlc.ogi.edu/spectra/hemoglobin/hemestruct/index.html, Accessed: 10/5/2009.

[78] A.N. Yaroslavsky, A.V. Priezzhev, J.R.I.V. Yaroslavsky, and H. Battarbee, "Optics of blood", in *Handbook of Optical Biomedical Diagnostics*, V.V. Tuchin, Ed., pp. 169–216. SPIE Publications, Bellingham, WA, 2002.

[79] S. Wray, M. Cope, D.T. Delpy, J.S. Wyatt, and E.O. Reynolds, "Characterization of the near infrared absorption spectra of cytochrome aa3 and haemoglobin for the non-invasive monitoring of cerebral oxygenation.", *Biochimica et Biophysica Acta - Bioenergetics*, vol. 933, no. 1, pp. 184–192, 1988.

[80] A.P. Harris, M.J. Sendak, R.T. Donham, M. Thomas, and D. Duncan, "Absorption characteristics of human fetal hemoglobin at wavelengths used in pulse oximetry", *Journal of Clinical Monitoring and Computing*, vol. 4, no. 3, pp. 175–177, 1987.

[81] S. Takatani and M.D. Graham, "Theoretical analysis of diffuse reflectance from a two-layer tissue model", *IEEE Transactions on Biomedical Engineering*, vol. 26, no. 12, pp. 656–664, 1979.

[82] D.W. Marquardt, "An algorithm for least-squares estimation of nonlinear parameters", *Journal of the Society for Industrial and Applied Mathematics*, vol. 11, no. 2, pp. 431–441, 1963.

[83] C. Harle-Bachor and P. Boukamp, "Telomerase activity in the regenerative basal layer of the epidermis in human skin and in immortal and carcinoma-derived skin keratinocytes", *Proceedings of the National Academy of Sciences*, vol. 93, no. 13, pp. 6476–6481, 1996.

[84] D. Yudovsky, A. Nouvong, K. Schomacker, and L Pilon, "Two-layer optical model of skin for early, non-invasive detection of wound development on the diabetic foot", in *Proceedings of the SPIE: Advanced Biomedical and Clinical Diagnostic Systems VIII*, 2010, vol. 7555, p. 7555.

[85] J.S. Vande Berg and R. Rudolph, "Pressure (decubitus) ulcer: variation in histopathology – a light and electron microscope study", *Human pathology*, vol. 26, no. 2, pp. 195–200, 1995.

[86] A.J. Boulton, P. Meneses, and W.J. Ennis, "Diabetic foot ulcers: A framework for prevention and care", *Wound Repair and Regeneration*, vol. 7, no. 1, pp. 7–16, 1999.